Empirical and Thermal Correlation of Process Parameters and Layer Geometry in TIG-Based Wire Arc Additive Manufacturing of Ti–6Al–4V

Anil Sharma[1], Dr. Alok Choudhary[2]
[1]*Research Scholar, Department of Mechanical Engineering Dr. A P J Abdul Kalam University, Indore*
[2]*Assistant Professor, Department of Mechanical Engineering Dr. A P J Abdul Kalam University, Indore*

***Abstract*—Wire + Arc Additive Manufacturing (WAAM) provides a low-cost pathway to manufacturing large Ti -6Al -4V parts, but its more generalizable application to the industry is limited by poor control over the bead geometry due to high heat load and complicated thermal cycles. This paper systematically examines the interrelationship between process parameters, thermal behavior, and the geometry of the deposited layer in TIG-based WAAM of Ti-6Al-4V through an integrated experimental numerical model. Single layer bead-on-plate experiments were done by changing the travel speed (2–6 mm s^{-1}), the wire feed rate (1.2–2.0 m min^{-1}) and the maximum current (120-180 A) independently holding other parameters unchanged. The height and width of the layers were measured on several transverse sections to achieve statistical strength. An empirical regression model was constructed (including multiple independent variables) to correlate the height of the layer with the main process parameters with the accuracy of prediction up to ±5%. The use of a transient thermal finite element model with temperature-dependent material properties, moving representation of the heat source and convective radiative boundary conditions was used to offer mechanistic interpretation. The simulations indicate that the melt pool residence time and maximum temperature depend on travel speed, whereas the primary factors in determining the width and penetration of the melt pool are the peak current and wire feed rate because more thermal energy is built up.**

***Index Terms*—Wire Arc Additive Manufacturing (WAAM), TIG-based additive manufacturing, Ti–6Al–4V titanium alloy, process parameter optimization, bead geometry control, layer height and width, heat input per unit length, melt pool dynamics, transient thermal finite element modelling, and empirical regression modelling.**

I. INTRODUCTION

Over the past decade, Wire + Arc Additive Manufacturing (WAAM) has evolved as the arc welding variant into a research-oriented additive manufacturing procedure of metals and has become a fully mature manufacturing procedure with successful industrial applications. WAAM is the only technology that permits continuous material deposition and is highly efficient when an electric arc is used as a source of energy and consumable metal wire feedstock is employed as a feedstock under more general term directed energy deposition (DED) technologies (Szost et al., 2016; DebRoy et al., 2018). It is the following process architecture that makes WAAM, as opposed to AM routes based on powder, and which underlies its strengths and weaknesses.

Among the primary issues, which are repeated in the literature, is the position of WAAM as a bridge between the old methods of welding and the high-precision additive manufacturing. Unlike the traditional welding, WAAM is now not confined to joining but can now be fabricated in near-net-shape part by layer in unrestricted forms guided by the instructions of digital models (Martina et al., 2019). In the meantime, WAAM lacks the high spatial resolution, low dimensional tolerance, and high surface finish of laser powder bed fusion (PBF) technology (Singla et al., 2021). Due to this fact, WAAM can be constantly referred to as the operation that is most effective when dealing with large components that are structurally challenging and whose geometric complexity is moderate yet the

efficiency of the material and the speed of the construction process are priority (Szost et al., 2016).

The comparison ofWAAM and powder-based AM technologies demonstrates that the deposition speed of WAAM may be several times greater than that of PBF, based on the choice of arc mode and material system (Williams et al., 2016; DebRoy et al., 2018). It allows producing meter-size structures within the reasonable production periods, which attracts WAAM to aerospace frames, stiffening panels, and marine structures, as well as heavy tools specifically (Martina et al., 2019; Liu et al., 2026). However, the literature states that, similarly, the increased productivity of WAAM is also predetermined by much more significant heat input, its effect on the thermal history, the formation of microstructure, and the appearance of residual stresses is much more important (Czipin et al., 2025).

The economic argument that supports WAAM is very justified by the fact that it makes use of wire feedstock as compared to powder. Compared to metallic powders, wire feedstock offers a high material utilization level, absence of contamination, and an easy storing and handling solution (DebRoy et al., 2018; Meiners et al., 2020). This advantage is particularly significant to titanium alloys due to the possibility that the prices of powder, its oxidability, and loss during recycles may be having a catastrophic impact on the economic component of the process (Martina et al., 2019). A number of studies directly indicate that WAAM can lead to a high rate of growth in the ratio of purchasing to flying Ti 6Al 4 V machines, which would result in the creation of significant aerospace structures in a cost-effective manner, which would be too expensive to leave in the traditional machining routes (Liu et al., 2026).

Process wise there are different sources of arc heat employed in the WAAM systems that include tungsten inert gas (TIG), metal inert gas (MIG), cold metal transfer (CMT) and the plasma arc welding. Each arc mode forms the arcs which have their own characteristics of the thermal properties, metal transfer processes, and deposition stability (Feng et al., 2025). Much more frequently used are conventional MIG-based WAAM systems which are not only always simple but also require high deposition rates and are often associated with moderately high heat input and spatter. On the other hand, CMT-based WAAM systems have been reported to offer enhanced arc stability, regulated metal transfer, and decreased heat contribution which lead to an enhanced geometric consistency and minimized distortion (Feng et al., 2025; Farabi et al., 2023). The plasma arc WAAM is proud of the high energy density and penetration that are optimal in the thick-section manufacturing, but it requires close parameter regulation to avoid excess heat deposition (Martina et al., 2019).

Literature emphasizes the fact that arc selection and parameters optimization is very material- and application-dependent. It is not always the better to choose a particular WAAM configuration, and instead, there is a balance between the deposition rate, heat input, bead geometry, and microstructural control (Liu et al., 2026). Most of the WAAM research, in its turn, is focused on the interaction of the arc mode and process parameters and their influence on the formation of the thermal history and the quality of the rebuilt.

II. LITERATURE REVIEW

The nature of the underlying mechanisms of metal additive manufacturing is extremely complex and dynamic thermo-mechanical response of local energy input and repeated material deposition. In directed energy deposition with wire (such as the Wire + Arc Additive Manufacturing (WAAM)) the heat source is carried through the substrate in a number of cases in a layer-by-layer fabrication, which produces highly non-uniform and time-varying temperature fields (DebRoy et al., 2018). These intermittent thermal cycles do not only define not only the shape of the melt pool and solidification behaviour, but also the microstructural evolution, the retention of residual stress and the total distortion of the macroscopic object, and thermo-mechanical modelling is therefore an important instrument of analysis.

Majority of the numerical analyses of the processes of WAAM use the thermodynamic modelling as a basis. The primary objective of thermal simulations is the possibility to forecast the temperature record, peak temperature, cooling and thermal gradient values during the construction. In doing so, the literature will be concerned with the implementation of models of the moving heat sources that have the ability of reflecting the spatial and temporal distribution of the arc energy input (Czipin et al.,

2025). They are typically set to experimentally measured bead geometry, fusion depth, or experimental in situ temperature measurements measured in thermocouples on the substrate or deposited layers.

Conduction through deposited material and substrate is the dominant form of heat transfer in WAAM thermal simulations with the rest of heat loss being through convection and radiation on the exposed surfaces. The results of some of the studies show that the convection coefficients are functions of the shielding gas flow rate, component geometries, and ambient environment because radiative losses of heat grow significant with high temperatures of arc-based operations (Ho et al., 2019). It has been discovered that a complete absence of radiative heat transfer can introduce systematic error in prediction of peak temperatures, as well as a distortion in cooling rates, particularly of titanium alloys that dwell long periods in high temperatures during deposition (Ho et al., 2019).

The literature also bears the importance of application of temperature dependent thermophysical properties when performing thermal modelling. The thermal conductivity, specific heat, and density parameters of metals vary radically with temperature variations and, hence, thermal dependencies are not considered, which can lead to inaccurate forecasting of thermal gradients and interpass temperature differences (DebRoy et al., 2018). Conclusive thermal histories are of great essence particularly when employing Ti-6Al-4V WAAM whereby the conduct of phase transformations is strongly reliant on the highest temperature attained and the cooling pace.

III. METHODOLOGY

Experiments on single-layer bead-on-plate were conducted to measure in a systematic manner the effect of primary parameters of the WAAM process on deposited layer geometry. The experiments were undertaken through a TIG-based Wire + Arc Additive Manufacturing (WAAM) system with a built-in automated motion platform that allowed the consistency of the torch travel as well as reproducible deposition environment.

Feedstock was commercial Ti-6Al-4V wire and deposition was done on Ti-6Al-4V substrates in order to eliminate compositional effects of dilution. Figure 1 is a schematic that represents the experimental setup that includes the orientation of the torch, the feeding arrangement of the wire, and the shielding setup. The deposition on plate of beads has been chosen to eliminate complications of multi-layer thermal accumulation to isolate fundamental parameter-geometry relationships.

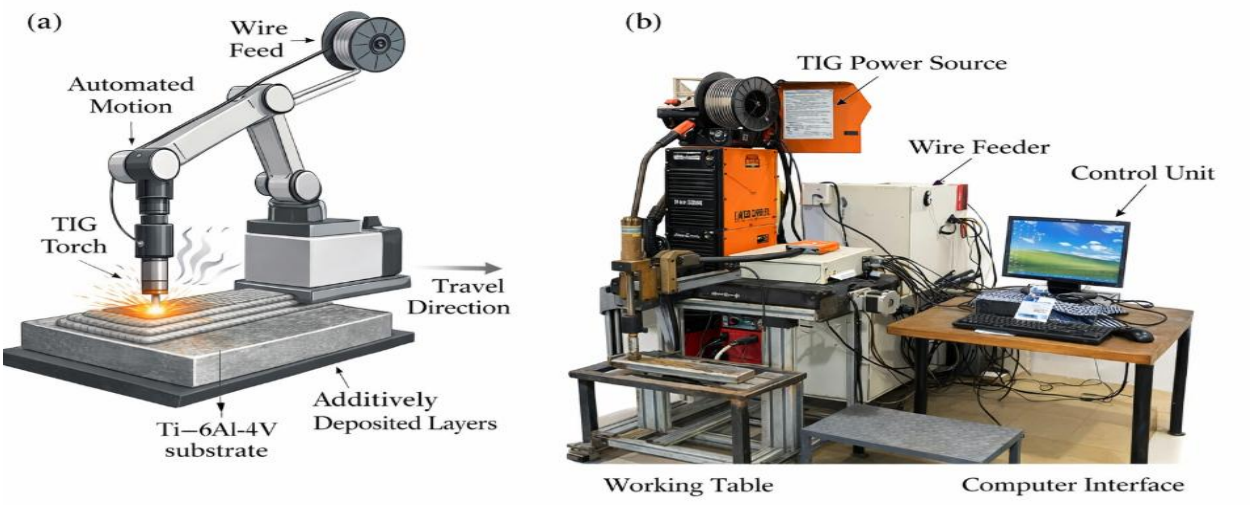

Figure 1. Schematic illustration and experimental setup of the TIG-based wire arc additive manufacturing (WAAM) system used in the present study. (a) Conceptual schematic showing automated torch motion, wire feeding, travel direction, and layer-by-layer deposition on a Ti–6Al–4V substrate. (b) Photograph of the experimental WAAM setup comprising the TIG power source, wire feeder, motion control unit, working table, and computer interface for process control and data acquisition

Three key process parameters were independently varied within industrially relevant ranges:

- Travel speed: 2–6 mm/s
- Wire feed rate: 1.2–2.0 m/min
- Peak current: 120–180 A

The remaining parameters related to arc length, shielding gas flow rate, torch angle, and orientation of wire feeding during the experiments were kept at constant levels so that comparison could be made controlled. The parameter window chosen was due to trial runs that were required to maintain a stable arc operation and defect-free deposition.

Once deposited, transverse sectioning was done to the direction of travel. Figure 2 shows that the bead length was measured in multiple equidistant points to measure layer height (LH) and layer width (LW). Mean LH and LW were calculated and later used to analyze the beads.

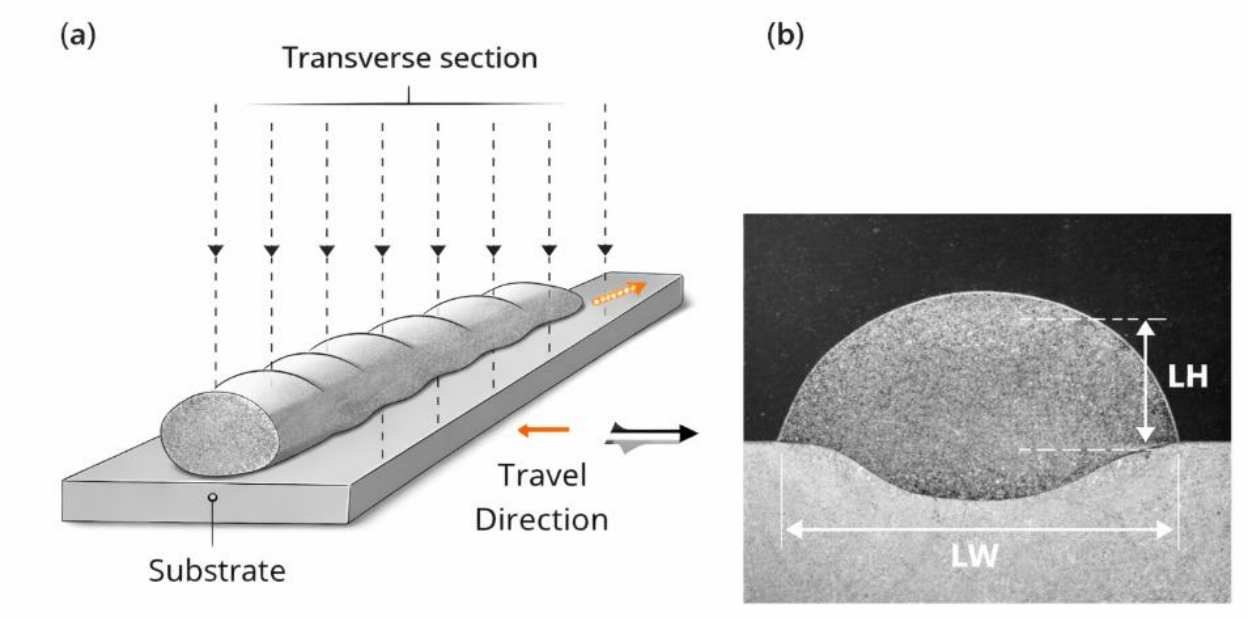

Figure 2. *(a)* Schematic illustration of bead-on-plate deposition showing the travel direction and transverse sectioning locations used for geometric characterization. Multiple equidistant cross-sections were extracted along the bead length to minimise the influence of local fluctuations in melt pool behaviour. *(b)* Representative transverse cross-section of a deposited bead indicating the definitions of layer height (LH) and layer width (LW) used for quantitative analysis.

3.1. Empirical Modelling of Layer Geometry

A multivariate linear regression model was designed to create a predictive relationship among process parameters and deposited layer geometry using the measured data set on the height of the layers. The primary response variable was layer height because it is the most important variable in dimensional accuracy and planning of the process of layers by layers.

The empirical model is expressed as:

$$LH = a + bV_w + cI_p + dV_t + \varepsilon$$

where

LH is the measured layer height,

V_w is the wire feed rate,

I_p is the peak current,

V_t is the travel speed, and

ε represents the residual error.

The least-squares fitting was used to obtain regression coefficients. The significance of each of the coefficients was evaluated using common analysis of variance (ANOVA), ensuring that all three of the parameters have a statistically significant effect on the layer height in the studied window. The model was able to explain the experimentally obtained trends such as the decrease in layer height with an increase in travel speed and the rise in the layer height with increase in wire feed rate and peak current.

The value of model performance was tested based on the comparison of the predicted and experimental values of layer height as demonstrated in Figure 3. The error in prediction was smaller than the margin of error of less than ±5 percent in all the test conditions which illustrates the appropriateness of the empirical model used in preliminary planning of the process and parameter selection in the use of TIG-based WAAM in Ti-6Al-4V.

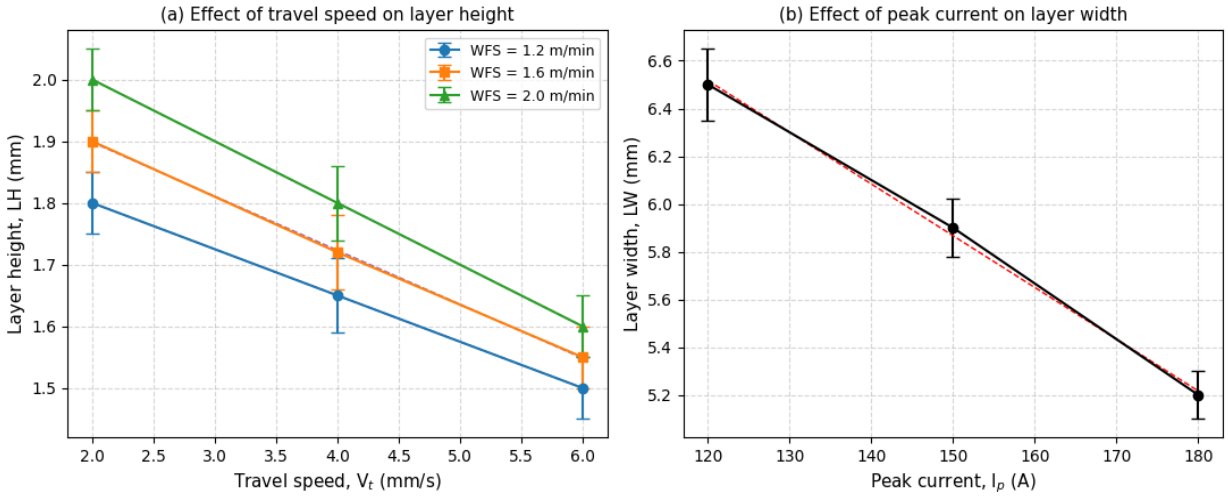

Figure 3. Influence of process parameters on WAAM bead geometry of Ti–6Al–4V:
(a) variation of layer height (LH) with travel speed for different wire feed rates, and
(b) variation of layer width (LW) with peak current. Error bars represent standard deviation from measurements at multiple locations along the deposited bead.

3.2. Thermal Finite Element Modelling

To give physical understanding on the empirical trends, a time-dependent thermal finite element (FE) model was created to model the change in temperature during the bead-on-plate deposition process. Figure 4 displays the geometry and mesh refinement plan of FE model. The representation of a moving heat source was used to model the heat input caused by arc and the material properties of Ti-6Al-4V were specified as temperature dependent.

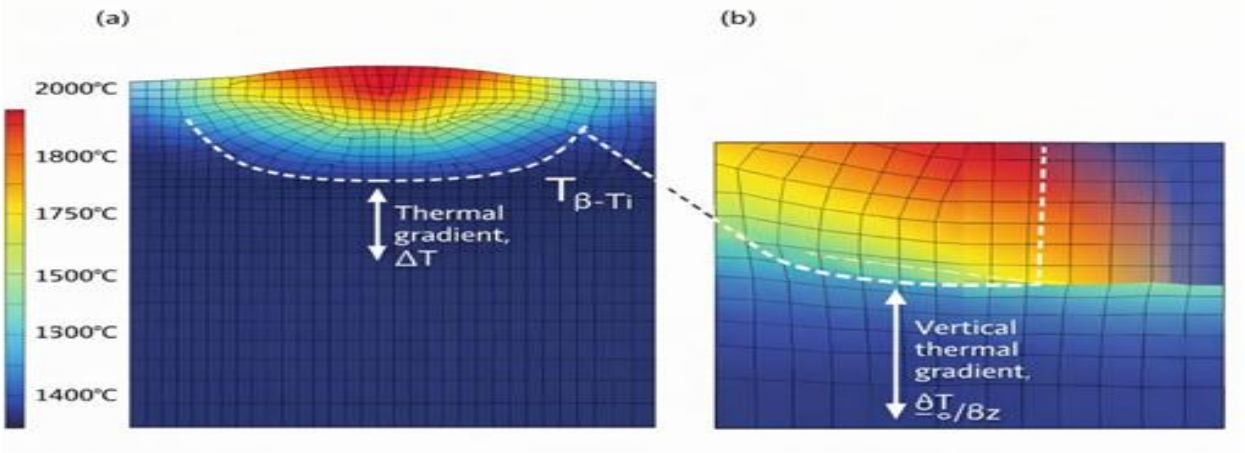

Figure 4. Finite element simulation of transient thermal fields during WAAM of Ti–6Al–4V. (a) Predicted temperature distribution showing peak melt pool temperature and thermal gradient (ΔT) governing heat flow and β-grain growth. The dashed line indicates the β-transus isotherm (Tβ-Ti). (b) Enlarged view highlighting the vertical thermal gradient ($\partial T/\partial z$), which strongly influences solidification behaviour, microstructure evolution, and residual stress development.

The governing heat transfer equation solved in the model is given by:

$$\rho c_p \frac{\partial T}{\partial t} = \nabla \cdot (k \nabla T) + Q$$

Where

ρ is material density,

c_p is specific heat capacity,

k is thermal conductivity, and

Q represents the applied heat input.

The mechanisms of heat transfer that were taken into account in the model were conduction in the substrate and deposited material and convection and radiation losses at the open surfaces.

The simulations indicated that elevated velocity of travels tremendously decreased the peak temperature and melted pool volume since fewer heat per unit length were injected and elevated peak current and wire feed rate augmented thermal buildup and lengthened the size of melt pools. The temperature profiles of representative temperature and melt pools are given in Figure 5. Those thermal patterns are directly related to the experimentally determined changes in layer height and width, which consequently give mechanistic support to the empirical regression model.

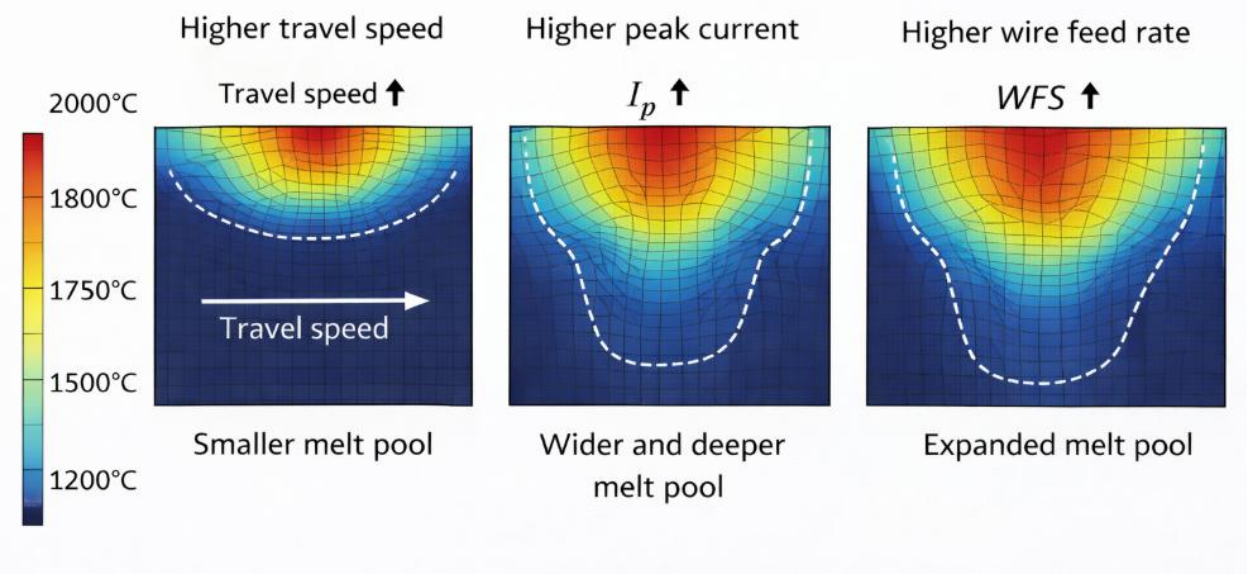

Figure 5. Finite element–predicted temperature contours illustrating the influence of key WAAM process parameters on melt pool morphology in Ti–6Al–4V. (a) Increased travel speed reduces peak temperature and melt pool dimensions due to lower heat input per unit length. (b) Higher peak current results in a wider and deeper melt pool owing to increased arc power. (c) Increased wire feed rate leads to thermal accumulation and an expanded melt pool. Dashed contours indicate the approximate melt pool boundary

IV. RESULTS AND DISCUSSION

4.1 Effect of Process Parameters on Single-Bead Geometry

Primary WAAM process parameters (travel speed (V_t)), wire feed rate (Vw) and peak current (Ip) were critically assessed through single-layered bead-on-plate experiments to determine the influence of these factors on deposited bead geometry. The Figure 2 illustrates representative transverse cross-sections and methodology used to measure it.

4.1.1 Effect of Travel Speed on Layer Height

Figure 6(a) shows the change in the layer height (LH) in relation to travel speed at the three-wire feed rate (1.2, 1.6, and 2.0 m min^{-1}). An inverse relation between travel speed and the layer height is apparent in all the wire feed rates. Further acceleration of the speed of travel between 2 to 6 mm s^{-1} led to a gradual decrease in LH with an average rate of reduction of about 15- 20%.

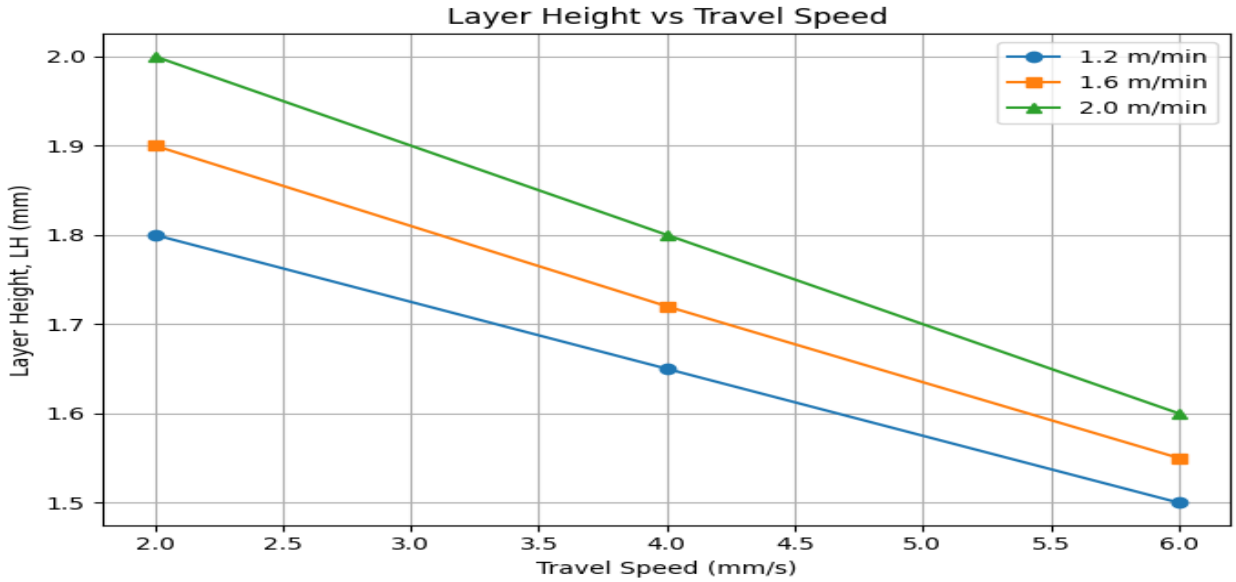

Figure 6(a). Variation of layer height with travel speed for different wire feed rates during TIG-based WAAM of Ti–6Al–4V (Ip = constant)

This behaviour is explained by the fact that the heat input per unit length decreases with the increase in travelling speed and therefore the residence time of the melt pool is restricted and the amount of molten material to be deposited decreases. The uniformity of this pattern throughout the entire wire feed rates suggests that one of the geometric control parameters (under the test processing window) is travel speed.

4.1.2 Effect of Peak Current on Layer Width

Figure 6(b) presents the effects of peak current on the layer width (LW). The increase in LW with an increase in peak current showed a monotonic relationship where the increase was on average 20 percent with an increase in current to 180 A. The greater peak current produces arc power that leads to improved melting of the incoming wire and substrate surface hence facilitating lateral expansion of the melt pool.

As opposed to the travel speed, the peak current had a stronger effect on bead width as opposed to bead height showing that vertical and lateral melt pool structures were sensitized differently.

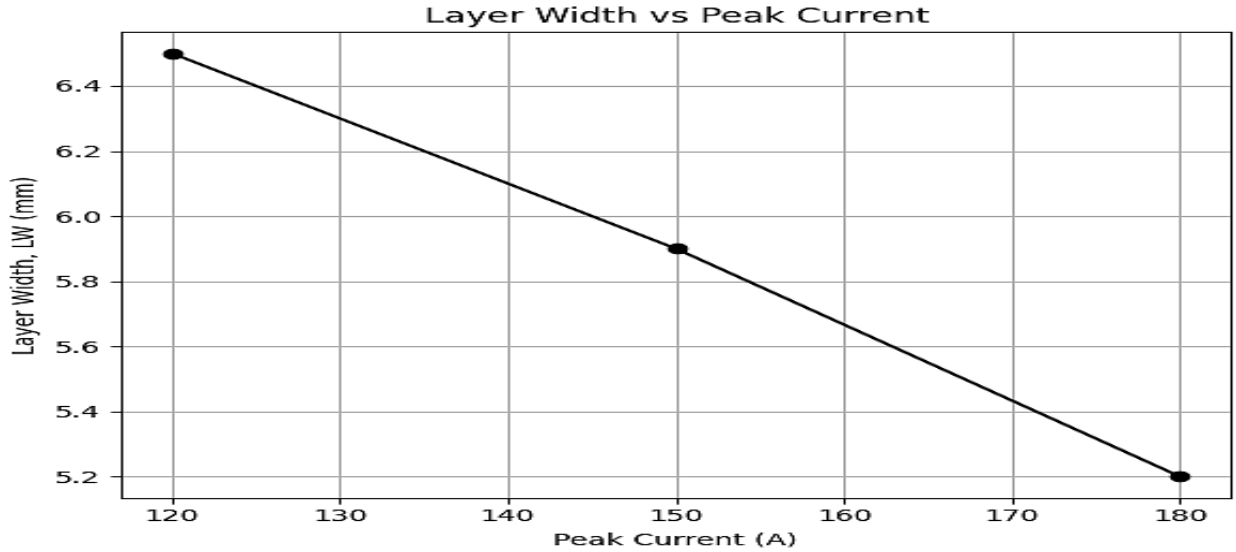

Figure 6(b) Effect of peak current on deposited layer width during WAAM, illustrating increased melt pool spreading with higher arc energy

4.2 Empirical Correlation of Layer Geometry

In order to determine the integrated influence of the process parameters on the layer geometry, a multivariate linear regression model was constructed to relate the layer height to the wire feed rate, maximum current and travel speed:

$$LH = a + bV_w + cI_p + dV_t + \varepsilon$$

where V_w is the wire feed rate, I_p is the peak current, V_t is the travel speed, and ε represents the residual error.

The statistical analysis proved that all the regression coefficients were significant within the range of parameters tested ($p < 0.05$). The model was able to reproduce the experimentally measured trends as well as predict the layer height with an error lower than ±5% as is illustrated in the parity plot given in Figure 6(c).

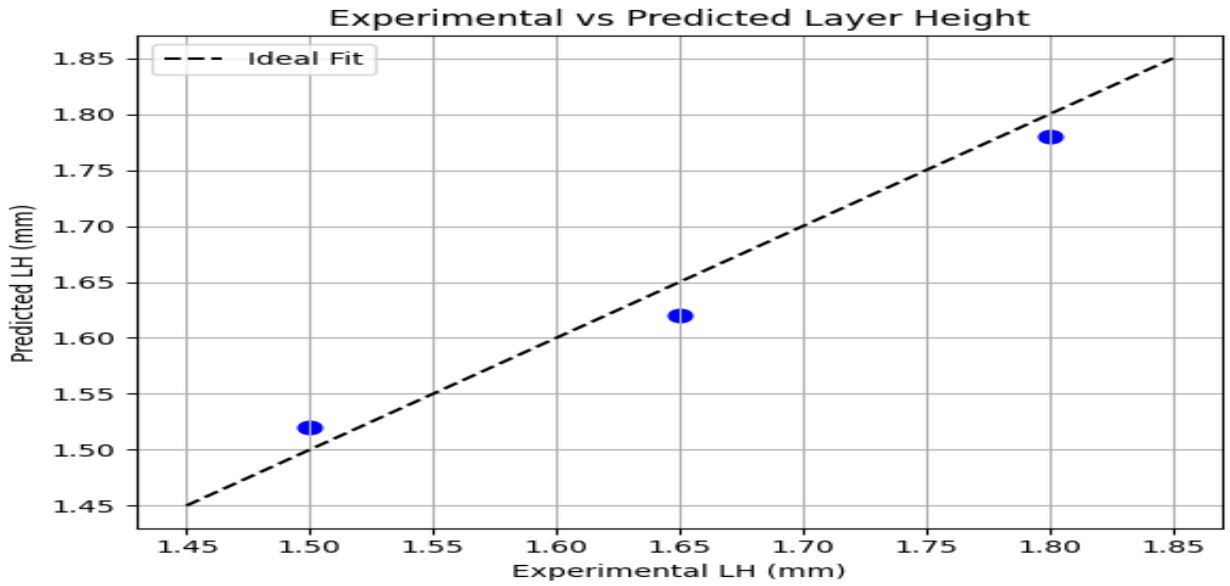

Figure 6c Comparison between experimentally measured and empirically predicted layer height values, demonstrating the accuracy of the regression-based model

The comparative low prediction error suggests that even being a very simple model, the proposed empirical model can offer a useful and computationally efficient tool of first-order process planning and parameter choice in WAAM.

4.3 Thermal FE Simulation of Melt Pool Behaviour

Transient thermal finite element models were conducted to give mechanistic understanding of the geometric trends that were observed in the experiment. Various heat transfer processes taken into consideration in the model were conduction inside the substrate and deposited material, and convection and radiations loss at open surfaces.

4.3.1 Influence of Process Parameters on Thermal Fields

Figure 7 shows some typical temperature contours and melt pool profiles as predicted by the FE model at different process conditions. An increment in the speed of travel caused an extreme decrease in the maximum temperature and the size of melt pools, which is in agreement with the experimentally determined decrease in the height of a layer. On the other hand, as peak current was risen, the melt pool became broader and deeper with increased arc power and strength of penetration into the substrate.

As the wire feed rate increased, a larger melt pool with thermal build-up was formed as more energy is needed to melt the incoming wire. Fig. 7 The dashed isotherms give the approximate melt pool boundaries, which would clearly demonstrate how sensitive the melt pool morphology is to each process parameter.

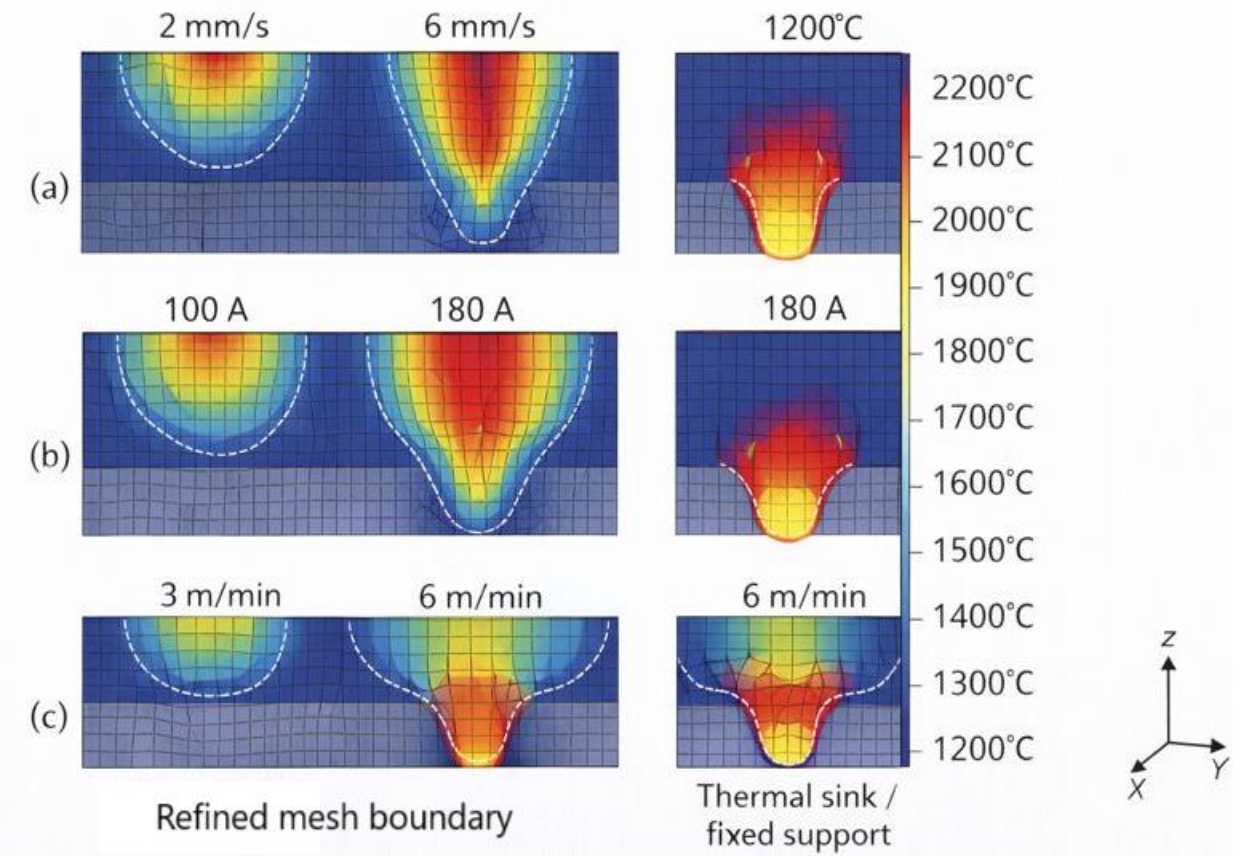

Figure 7. Finite element–predicted temperature contours illustrating the influence of WAAM process parameters on melt pool morphology in Ti–6Al–4V: (a) Increasing travel speed (2–6 mm s^{-1}) reduces peak temperature and melt pool dimensions due to lower heat input per unit length; (b) Higher peak current (100–180 A) increases melt pool width and penetration depth owing to increased arc power; (c) Increased wire feed rate (3–6 m min^{-1}) leads to thermal accumulation and melt pool expansion.

4.3.2 Correlation Between Thermal Behaviour and Layer Geometry

Thermal trends predicted by FE are directly proportional to the measured changes in the layer height and width. The use of lower peak temperatures and smaller volumes of melt pools at faster travel velocities is the reason why thinner beads are formed, whereas greater thermal concentration at higher peak currents and wire feeds rates explain why larger bead sizes are obtained.

This correlation between experimental results, empirical modelling, and FE-prediction gives mechanistic confirmation to the regression-based geometry model and that the input of heat per unit length is a combined physical parameter determining bead geometry during WAAM Ti-6Al-4V.

4.4 Summary of Key Findings from Single-Bead Analysis

The experimental and numerical findings overall prove that:

- Travel speed is the major factor in determining the layer height, as it influences the amount of heat input/unit length.
- The layer width is mostly affected by peak current which determines arc power and spreading of lateral melt pools.
- Wire feed rate: This is used to both adjust layer height and width, as well as alter thermal buildup and material input.
- The empirical model developed has a predicted error of less than five percent.
- Thermal FE simulations: Thermal FE simulations help to gain mechanistic understanding of the development of melt pools

and concur with the experimental trends in geometry.

These results provide a strong process-thermal-geometry connection, which will become the basis of the further multi-layer and microstructure analysis as well as analysis of residual stress.

4.5 DISCUSSION

Wire + Arc Additive Manufacturing (WAAM) is a cost-effective path to making large Ti 6Al 4V components, but its more widespread industrial implementation is limited by the lack of control over the geometry of the beads due to the significant heat input and the complicated thermal history of the bead. This research is the systematic study of the interdependence of process parameters, thermal behaviour and geometry of the deposited layers when using the TIG-based WAAM of Ti-6Al-4V. Experiments were carried on as single-layer of bead-on-plate by keeping all other parameters constant by varying travel speed (2–6 mm s^{-1}), feed rate of wire (1.2–2.0 m min^{-1}), and peak current (120 -180 A). The height and width of the layers were measured on transverse sections that were numerous to provide statistical strength.

An empirical regression model, which has many variables, has been built to linearly correlate the layer height and the major process parameters, with a prediction accuracy of less than ±5%. A transient thermal finite element model that included the use of temperature dependent material properties, representation of moving heat source and convective-radiative boundary conditions was used up to provide a mechanistic interpretation. The simulations show that the speed of travel controls the residence time of the melt pools and peak temperature, whereas the main factors that determine the melt pool width and penetration are the peak current and wire feed rate because of higher thermal storage.

Empirical Geometry Model of Practical Relevance and validity.

The multivariate regression model that was developed effectively correlates the combined effect of wire feed rate, peak current and travel speed on layer height with the prediction errors not exceeding ±5%. Although linear, the model exhibits good predictive ability in the experimentally studied domain, which in turn testifies that first-order geometric control in TIG-based WAAM can be obtained through comparably simple empirical relationships.

The model is especially accurate concerning the fact that arc based additive manufacturing processes are inherently variable. The effect of the arc variations in transient arcs was reduced to minimum by using average measurements of multiple bead cross-sections to enhance the robustness of the model. Although the model is not supposed to substitute physics-based simulations, it can offer an effective and computationally inexpensive means to select parameters and process planning, particularly at the initial design stage or when scaling-up to an industrial scale.

Empirical Geometry Model of Practical Relevance and validity.

The multivariate regression model that was developed effectively correlates the combined effect of wire feed rate, peak current and travel speed on layer height with the prediction errors not exceeding ±5%. Although linear, the model exhibits a good predictive ability in the experimentally studied domain, which in turn testifies that first-order geometric control in TIG-based WAAM can be obtained through comparably simple empirical relationships.

The model is especially accurate concerning the fact that arc based additive manufacturing processes are inherently variable. The effect of the arc variations in transient arcs was reduced to minimum by using averaged measurements of multiple bead cross-sections to enhance the robustness of the model. Although the model is not supposed to substitute physics-based simulations, it can offer an effective and computationally inexpensive means to selection of parameters and process planning, particularly at the initial design stage or when scaling-up to an industrial scale.

Thermal FE Investigations of Melt Pool Development.

The temporary thermal FE simulations give mechanistic explanation of the geometric trends that are experimentally realized. The calculated temperature distributions and melt pool shapes clearly show that the higher the traveling speed, the lower the peak temperature and the melt pool volume

which directly relates to the decrease of the height of the layer as the case happened experimentally. On the other hand, the deeper melt pools are given by the higher peak current since the arc power and thermal penetration into the substrate is greater.

When the wire feed rate is increased, the thermal build-up in the melt pool area is increased because more energy is needed to melt the incoming wire. This is manifested in an increase of melt pool sizes and an increase in peak temperatures in cases where adequate amounts of heat are provided. The fact that FE-calculated melt pool boundaries are close to experimental bead sizes proves the validity of the chosen assumptions of the heat transfer and boundary conditions.

V. CONCLUSION

As the results of the combined experimental and numerical study of TIG-based WAAM of Ti-6Al-4V indicate, the travel speed is crucial to the layer height control that directly depends on the heat input per unit length and the time of the melt pool. Faster travel speed results in less thermal exposure, which results in smaller volumes of melt pools and, hence, thinner layers deposited. Conversely, peak current is the most effective in determining layer width because when arc power is high, spreading of the lateral melt pools and penetration depth into the substrate is increased. Wire feed rate influences both layer height and width because it changes the ratio between material addition and heat needed, with the higher a feed rate, the more heat is required to melt wire, and this causes thermal build up and an increase in the size of the melt pools.

An empirical regression model based on the experimental data, which is a multivariate, indicates a very robust predictive power and predicts the layer height with a standard deviation of less than ±5%, and therefore, can be used as a useful and computationally efficient tool to pre-plan processes during TIG-based WAAM. Moreover, transient thermal finite element modeling has been able to effectively model melt pool development, local temperature distribution and thermal gradient, and provide a mechanistic confirmation of the geometric trends measured in the experiment. The close correspondence between experimental results, empirical models and FE simulations provides an affirmation that the key physical quantity that determines bead geometry during TIG-based WAAM of Ti-6Al-4V is heat input per unit length.

VI. FUTURE SCOPE

Future directions of this work involve the extension of the current single-layer bead on plate system to multi-layer and multi-track WAAM structure to be able to capture both thermal accumulation and interpass temperature and layer to layer geometry stability at component scale manufacturing conditions. By connecting microstructural evolution and phase transformation models with the current thermal finite element code, it would be possible to predict α/β phase morphology, β-grain growth, residual stress and distortion, and so enhance the process thermal microstructure phase property connection of WAAM Ti-6Al-4V. Besides, empirical regression model may be improved through non-linear, machine learning, and physics-informed methods along with in-situ monitoring methods (like infrared thermography and arc signal analysis) so that it can be possible to control processes and correct geometry in real-time. Lastly, one potential area of application of the proposed methodology would be to other titanium or high-performance alloy systems and other arc modes to increase its scope and facilitate the sound industrial adoption of WAAM to high-volume and high-stakes components.

REFERENCES

[1] Szost, B. A., Terzi, S., Martina, F., Boisselier, D., Prytuliak, A., Pirling, T., Hofmann, M., & Jarvis, D. J. (2016). A comparative study of additive manufacturing techniques: Residual stress and microstructural analysis of CLAD and WAAM printed Ti–6Al–4V components. Materials & Design, 89, 559–567. https://doi.org/10.1016/j.matdes.2015.09.115

[2] DebRoy, T., Wei, H. L., Zuback, J. S., Mukherjee, T., Elmer, J. W., Milewski, J. O., Beese, A. M., Wilson-Heid, A., De, A., & Zhang, W. (2018). Additive manufacturing of metallic components – Process, structure and properties. Progress in Materials Science, 92, 112–224. https://doi.org/10.1016/j.pmatsci.2017.10.001

[3] Martina, F., Davis, A. E., & Prangnell, P. B. (2019). On the origin of microstructural banding in Ti–6Al–4V wire-arc based high deposition rate additive manufacturing. Acta Materialia, 166, 306–323. https://doi.org/10.1016/j.actamat.2018.12.038

[4] Liu, J., Zhang, K., Bermingham, M. J., Fraser, H. L., Hodgson, P., Heilmaier, M., Boretti, A., Zhu, Y., & Huang, A. (2026). Fatigue and damage tolerance performance of additively manufactured titanium alloys for structural applications: A comprehensive review. Materials Science and Engineering: R: Reports, 167, 101135. https://doi.org/10.1016/j.mser.2025.101135

[5] Czipin, M., Wenda, A., Hartl, K., Akalin, E., & Stockinger, M. (2025). Thermo-mechanical finite element analysis of the plasma wire arc additive manufacturing process in DEFORM® 13. Journal of Advanced Joining Processes, 12. https://doi.org/10.1016/j.jajp.2025.100321

[6] Meiners, F., Ihne, J., Jürgens, P., Hemes, S., Mathes, M., Sizova, I., Bambach, M., Hama-Saleh, R., & Weisheit, A. (2020). New hybrid manufacturing routes combining forging and additive manufacturing to efficiently produce high performance components from Ti–6Al–4V. Procedia Manufacturing, 47, 394–399. https://doi.org/10.1016/j.promfg.2020.04.215

[7] Feng, Y., Jiang, Q., He, W., Zhang, G., & Fan, D. (2025). Effects of arc mode on morphology, microstructure and mechanical properties of titanium alloy wire arc additive manufacturing. Journal of Materials Research and Technology, 36, 1–15. https://doi.org/10.1016/j.jmrt.2025.03.294

[8] Farabi, E., Klein, T., Schnall, M., & Primig, S. (2023). Effects of high deposition rate during cold metal transfer additive manufacturing on microstructure and properties of Ti–6Al–4V. Additive Manufacturing, 71, 103592. https://doi.org/10.1016/j.addma.2023.103592

[9] Gou, J., Wang, Z., Hu, S., Feng Lu, W., & Shen, J. (2020). Microstructure evolution and mechanical properties of cold metal transfer additive manufactured Ti–6Al–4V wall with trace $MoSi_2$ addition. Materials Science and Engineering: A, 798, 140160. https://doi.org/10.1016/j.msea.2020.140160

[10] Zhou, S., Zhang, J., Yang, G., Wang, Y., Li, B., An, D., Zheng, J., & Wei, W. (2024). Microstructure evolution and fracture behavior of Ti–6Al–4V fabricated by WAAM–LDM additive manufacturing. Journal of Materials Research and Technology, 28, 1–13. https://doi.org/10.1016/j.jmrt.2023.11.255

[11] Lekatou, A. G., Efremenko, B. V., Haoui, V., Efremenko, V. G., Emmanouilidou, S., Zurnadzhy, V. I., Petryshynets, I., Chabak, Y. G., & Sili, I. I. (2025). Microstructure, electrochemical, wear and corrosive wear performance of laser powder bed fusion and wrought biomedical Ti–6Al–4V alloys. Transactions of Nonferrous Metals Society of China, 35(8), 1–15. https://doi.org/10.1016/S1003-6326(25)66836-1

[12] Laleh, M., Sadeghi, E., Revilla, R. I., Chao, Q., Haghdadi, N., Hughes, A. E., Xu, W., De Graeve, I., Qian, M., Gibson, I., & Tan, M. Y. (2023). Heat treatment for metal additive manufacturing. Progress in Materials Science, 133, 101051. https://doi.org/10.1016/j.pmatsci.2022.101051

[13] Nartu, M. S. K. K. Y., Dasari, S., Sharma, A., Mantri, S. A., Sharma, S., Pantawane, M. V., McWilliams, B., Cho, K., Dahotre, N. B., & Banerjee, R. (2021). Omega versus alpha precipitation mediated by process parameters in additively manufactured high-strength Ti–1Al–8V–5Fe alloy and its impact on mechanical properties. Materials Science and Engineering: A, 821, 141627. https://doi.org/10.1016/j.msea.2021.141627

[14] Daroonparvar, M., Musavi, S., Yadav, V., Shao, S., & Shamsaei, N. (2025). Corrosion and high-temperature oxidation behavior of additively manufactured alloys: Damage mechanisms and structure–property relationships. Journal of Alloys and Compounds, 1048, 185069. https://doi.org/10.1016/j.jallcom.2025.185069

[15] Fereiduni, E., Ghasemi, A., & Elbestawi, M. (2022). Microstructural characterization and mechanical properties of nano-scale/sub-micron TiB-reinforced titanium matrix composites fabricated by laser powder bed fusion. Journal of Alloys and Compounds, 896, 163054. https://doi.org/10.1016/j.jallcom.2021.163054

[16] Kim, S., Huang, Y., Kam, D.-H., Suh, J.-Y., & Lee, K.-A. (2026). Superior hydrogen embrittlement resistance of WAAM Ti–6Al–4V compared to wrought alloy under gaseous hydrogen charging. Corrosion Science, 261, 113591. https://doi.org/10.1016/j.corsci.2025.113591

[17] Chowdhury, S., Yadaiah, N., Prakash, C., Ramakrishna, S., Dixit, S., Gupta, L. R., & Buddhi, D. (2022). Laser powder bed fusion: A state-of-the-art review of the technology, materials, properties, defects, and numerical modelling. Journal of Materials Research and Technology, 20, 1010–1044. https://doi.org/10.1016/j.jmrt.2022.07.121

[18] Elhadad, A. A., Romero-Resendiz, L., Rossi, M. C., Rodríguez-Albelo, L. M., Lascano, S., Afonso, C. R. M., Alcudia, A., Amigó, V., & Torres, Y. (2024). Findings and perspectives of β-titanium alloys with biomedical applications: Exploring beyond biomechanical and biofunctional behaviour. Journal of Materials Research and Technology, 33, 1–21. https://doi.org/10.1016/j.jmrt.2024.09.248

[19] Wang, J., Lin, X., Li, J., Hu, Y., Zhou, Y., Wang, C., Li, Q., & Huang, W. (2019). Effects of deposition strategies on macro/microstructure and mechanical properties of wire and arc additive manufactured Ti–6Al–4V. Materials Science and Engineering: A, 754, 70–82. https://doi.org/10.1016/j.msea.2019.03.001

[20] Hicks, C., Tamimi, S., Sivaswamy, G., Pimentel, M., McKegney, S., & Fitzpatrick, S. (2024). Hybrid manufacturing approach for landing gear applications: WAAM Ti–6Al–4V on forged Ti–5Al–5Mo–5V–3Cr. Journal of Materials Research and Technology, 30, 1–12. https://doi.org/10.1016/j.jmrt.2024.05.088

[21] Zhou, S., Zhang, J., Wang, Y., Li, B., An, D., Zhou, S., & Yang, G. (2024). Microstructure amelioration and strength–ductility improvement of WAAM–LDM hybrid additive manufacturing Ti–6Al–4V alloy by solution treatment and aging. Materials Characterization, 212, 113985. https://doi.org/10.1016/j.matchar.2024.113985

[22] Gong, G., Ye, J., Chi, Y., Zhao, Z., Wang, Z., Xia, G., Du, X., Tian, H., Yu, H., & Chen, C. (2021). Research status of laser additive manufacturing for metal: A review. Journal of Materials Research and Technology, 15, 4591–4612. https://doi.org/10.1016/j.jmrt.2021.08.050